Bi_m^+ ion beam patterning of germanium surfaces at different temperatures and ion fluence

Angélica Guadalupe Hernández[a] and Yuriy Kudriavtsev
Solid State Electronics Section, Electrical Engineering Department, CINVESTAV-IPN, Av. IPN n. 2508, Col. San Pedro Zacatenco, D.F. C.P. 07360, Mexico

(Received 4 August 2016; accepted 31 October 2016; published 10 November 2016)

Studies of pattern formation on variable-temperature Ge targets by ion beam sputtering are presented. A high-energy heavy polyatomic bismuth ion beam was used to reveal the effect of thermal spikes in the dynamics of pattern formation. By varying the target temperature in the range from 123 to 773 K, different morphologies of the irradiated surfaces were obtained. A smooth surface was observed for a target temperature of 123 K. Sputtering at a target temperature between 300 and 573 K gave rise to poorly oriented dot patterns and resulted in a checkerboard pattern at a target temperature of 773 K. Mechanisms of surface patterning under ion irradiation are discussed. [http://dx.doi.org/10.1116/1.4967697]

I. INTRODUCTION

Ion beam sputtering (IBS) is defined as the process in which atoms are ejected from a solid surface due to energetic particle bombardment. It is well known that this phenomenon has a wide range of technological applications.[1] Recently, IBS has been used for the production of nanostructured surfaces. The technique is becoming more and more attractive because complex methods of fabrication are not required.[2] Ion irradiation typically gives rise to four different types of surface morphologies: ripples, dots, pyramids, and smooth surfaces. A smooth surface is preferable for surface analysis by secondary ion mass spectroscopy (SIMS) and also by other analytical techniques based on ion sputtering[3] (auger electron spectroscopy, X-ray photoelectron spectroscopy, and ion scattering spectroscopy). The ripple pattern formation has been thoroughly studied. It can be well described by the Bradley–Harper theory,[4] including its additional modifications that consider the nonlinear effects at sputtering.[5] The ripple pattern is observed for almost all materials, including different metals and almost any semiconductor, though the experimental conditions can appreciably differ.[6–10] The nanodot pattern with a hexagonal array was obtained for the first time by Fascko in the ion sputtering experiment with GaSb,[11] and later, it was reported for different materials.[12] Its dynamics of formation was modeled by including a large value of the damping parameter describing the additional effect, leading to a hexagonal order into the Kuramoto–Sivashinsky equation (K-S).[13]

The nanopatterning on germanium (Ge) surfaces was studied in the search for the possibility to fabricate Ge quantum dots by means of a relatively simple procedure. Even when Ge has an indirect band gap, the quantum confinement effect causes light emission in this material,[14] and the luminescence properties can be applied to fabrication of light emitting devices. Ripple and dot nanopatterns were observed on Ge surfaces when the incident ion mass was greater than the mass of the Ge target atom.[15] Well-ordered ripples were observed after Xe^+ and Kr^+ irradiation with a low energy beam under an oblique incidence at room temperature (RT). Teichmann *et al.*[15] reported that the ripple pattern amplitude and regularity increased with time (pattern coarsening). In addition, Mollick *et al.* fabricated a defect-free ripple pattern on a Ge surface by an Au^- ion beam with an angle of incidence of 60° with respect to the surface normal when the energy beam was 26 keV. The mean wavelength of the ripple pattern varied according to the ion fluence from 280 to 370 nm.[16]

Ziberi *et al.* obtained a dot pattern on Ge surfaces after Xe^+ irradiation with an energy of 2 keV at room temperature under a normal incidence without sample rotation.[12] For an off-normal ion incidence, the dot structures evolved into a highly ordered ripple pattern, and when the angle of incidence was between 15° and 20°, a dot pattern with a hexagonal array was observed. Ou *et al.* have reported a novel crystalline checkerboard pattern on Ge surfaces at a normal incidence of Ar^+ ions with a 1-keV energy when the target temperature was above 528 K.[17] Same type of pattern was obtained by Chowdhury *et al.*[18] on Ge at 573 K after irradiation at normal incidence with Ar^+ ions with energy of only 30 eV.

Bischoff *et al.*[19–21] along with Böttger *et al.*[22–25] investigated the Ge surfaces after irradiation with Bi monomer and cluster ions. The experimental parameters of sputtering as target temperature, ion energy, and angle of incidence were varied in their work. It was remarkable that the surface morphology varies from a smooth surface to nanodots, holes, ripples, or sponge patterns accordingly to the experimental conditions. The spongelike pattern was observed for Bi_1^+ irradiation at normal incidence with energies between 20 and 30 keV; meanwhile, a dot pattern was found after the irradiation with heavy cluster ions of Bi_n^{m+}.

The dynamics of ripple and dot patterns formation has been widely discussed in the literature. The theoretical studies have been based on the approach of the linear collision cascade of sputtering[4,13,26] and recently on the thermal spike regime[27] where the formation of local melted zones plays a key role in dot pattern formation.[19–25,42]

In this work, we focus our attention on the thermal spike regime which is achieved when the temperature of a dense

[a]Electronic mail: ghernandez@cinvestav.mx

target is increased and heavy and (or) cluster ions with energies above 25 keV are used.[28] A thermal spike is characterized by the formation of a transient dense region in the cascade zone where most atoms are in motion[29] and by an abrupt temperature rise along with the transient dense collision cascade.

Samartsev *et al.*[28] studied the yields and emission velocity of sputtered indium (In) neutral atoms and dimers (In_2) under polyatomic gold (Au) bombardment (Au^-, Au_2^-, and Au_3^-). Two different ion beam energies, 5 and 10 keV, were used. The authors concluded that the thermal spike regime was realized already at an ion energy of 10 keV if Au_2^- or Au_3^- clusters were used for sputtering.

In our study, we compared surface patterning for linear collision cascade, the thermal spike sputtering regimes and an "intermediate" regime, when we suggest a mix of linear cascades formed by Bi_1^+ ions, and thermal spikes excited by Bi_3^+ ions with 30 and 60 keV ion energies. To change these three regimes, we used additional heating of the target.

II. EXPERIMENT

The samples approximately $1 \times 1\,cm^2$ in size were cut from standard 2 in. wafers and cleaned in an ultrasonic bath with ethanol during 5 min. Then, they were blown with nitrogen and placed into a vacuum chamber (load–lock). A controlled ion irradiation was carried out by a TOF-SIMS-5 secondary ion mass spectrometer from ION-TOF at 127, 300, 373, 573, and 773 K. A polyatomic Bi_m^+ ion beam with a mix of Bi_1^+, Bi_2^+, Bi_3^+, and Bi_3^{++} ions, the relative intensities of the ions in the beam being 100:29.3:24.7:24.4, respectively, was used (the so-called DC mode of bismuth LMIG). The ion beam energy was 30 keV (for the Bi_3^{++}, the energy ion was 60 keV). The ion bombardment was performed at a 45° incidence angle with a constant ion beam current of 30 nA. Squares of $300 \times 300\ \mu m$ have been written in a frame of 128 pixels by a mean spot size 3–5 μm with different sputtering times under ultrahigh vacuum conditions (the base pressure was $\sim 10^{-9}$ mbar). The pixel dwell time was fixed to be 100 μs. The ion fluence was varied from 1.3×10^{16} to 3.8×10^{17} ions/cm^2, which corresponded to an erosion time of 60 and 1800 s, respectively. To control the temperature, we used an Eurotherm (a G sample holder from Ion-Tof GmbH) controller for heating and cooling. Liquid nitrogen (LN) was used for cooling.

After ion irradiation, the surface morphology was investigated by atomic force microscopy (AFM) using a Solver Next instrument from NT-MDT. The measurements were carried out in the tapping mode to analyze the 3D surface relief. All the measurements were conducted in air by using silicon tips with a tip curvature radius of about 10 nm. The AFM measurements were performed for different scan sizes from 2×2 up to $50 \times 50\ \mu m^2$ with a resolution of 512×512 pixels and scanning frequency of 3 Hz. The surface roughness statistics and the surface topography were analyzed in an area of $5 \times 5\ \mu m^2$. The root-mean square (RMS) roughness of Ge before IBS was found to be 1.42 nm. The one dimensional power spectral density function was obtained from the fast Fourier transformed (FFT) height profile of images with a size of $2 \times 2\ \mu m^2$.

The Raman spectra were obtained by a confocal Raman NTEGRA Spectra instrument from NT-MDT with a laser excitation of 532 nm and 100× objective. The exposure time was 10 s, and the CCD was cooled down to 213 K.

III. RESULTS AND DISCUSSION

A. Ion bombardment at low temperatures

Figure 1 shows the Ge surface after bismuth ion irradiation. The substrate was cooled with LN to 123 K and irradiated by using two different ion fluences: 1.3×10^{18} ions/cm^2 [Fig. 1(a)] and 3.8×10^{18} ions/cm^2 [Fig. 1(b)]. As the ion fluence increases, there is a slight increase in the roughness

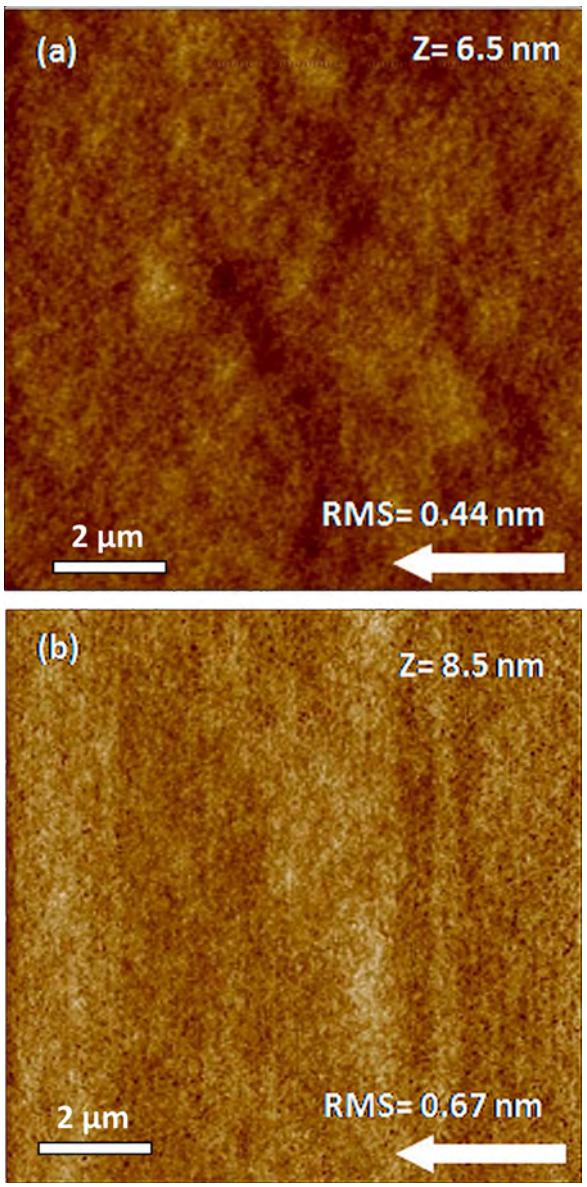

FIG. 1. (Color online) AFM images of $10 \times 10\ \mu m^2$ of Ge after bismuth irradiation at substrate temperature of 123 K for $E_{ion} = 30$ keV and $\theta_{inc} = 45°$. The ion fluence is different for each case: 1.3×10^{18} ions/cm^2 (a) and 3.8×10^{18} ions/cm^2 (b). The white arrow shows the projected ion beam direction. The RMS roughness was measured in a $5 \times 5\ \mu m^2$ area.

from 0.44 to 0.67 nm. However, the surface remains smooth in both cases, and the roughness is lower than before ion bombardment (1.42 nm).

Earlier, Teichmann *et al*. observed smooth Ge surfaces after ion irradiation when the incident ion mass was lower than the mass of the Ge target atom, irrespective of the angle of incidence and also for a Kr^+ ion beam with an energy of 1.2 keV at normal incidence, 20° and 60°.[15] In our study, we observed the smoothing effect at Ge surfaces regardless of the ion fluence. From our point of view the smoothing effect at low target temperature is attributed to the surface amorphization caused by ion irradiation and to a radical decrease in the diffusivity of both adatoms and vacancies, i.e., there is no any preferential orientation for the diffusion of surface atoms and vacancies,[18] and their diffusion length is too small to generate any self-organizing structures. The amorphization of the surface we confirmed by the Raman spectra is presented below. Smoothing of surfaces after IBS at low-temperature substrate was also observed for compound semiconductors,[30] and it was shown to be a determining factor for the SIMS depth profile improvement. A smooth surface is preferable for preventing the surface segregation effect in the study of ultranarrow delta layers, quantum wells, and shallow implanted layers[30] by SIMS and related analytical techniques. Sample cooling seems to be a good method for the preparation of smooth surfaces by FIB.

B. Ion bombardment at room temperature

Figure 2 shows germanium surfaces after bismuth ion irradiation at room temperatures for different ion fluences. The white arrow indicates the direction of the projected ion beam. The top image shows the irradiated area of 20 × 20 μm^2 where it is possible to observe the formation of "islands of dots." The surface bombarded with an ion fluence of 6.3×10^{16} ions/cm^2 [Fig. 2(a)] demonstrates an early stage of the dot agglomeration. The surface irradiated with an ion fluence of 1.3×10^{17} ions/cm^2 [Fig. 2(b)] is characterized by a smaller size of the islands of dots as compared with the surface bombarded with higher ion fluences [Figs. 2(c) and 2(d)]. The bottom panels show magnified islands of dots. The bottom left panel shows the AFM images with a size of 2 × 2 μm^2, and the bottom right panel shows the corresponding FFT height profile. In Fig. 2(a), the FFT image demonstrates a ringlike shape which results from a random (isotropic) distribution of nanodots.[12] If an ion fluence of 2.5×10^{17} ions/cm^2 is used, the agglomerates in the form of dots occupying a very small region [Fig. 2(c)] result. However, these dots are neither periodic nor preferentially oriented. Its low symmetry in the FFT image points to a preferential orientation of the agglomerates of nanodots, but there is still no distinct (well pronounced) pattern. The AFM image shows that the dots have a tendency to agglomerate in a circular island. The average dot size is 44.9 nm. When the ion fluence grows to 3.8×10^{17} ions/cm^2 [Fig. 2(d)], the average dot size increases to 49.8 nm. This is consistent with the dot behavior reported earlier in the literature.[31] The increase in the ion fluence gives rise to the formation of dot structures, but no regular pattern is observed in both the AFM image and Fourier space. At this stage, the ion bombardment at room temperature forms poorly ordered agglomerates of nanodots with a tendency to a preferential orientation rather than a well-defined pattern.

The increase in the size and dimensions of dot islands is due to the predominant roughness coarsening mechanism. The impinging Bi^+ ions reflected from islands contribute to the erosion enhancement in the island itself, resulting in coarsening of the structures (dot size as well).[32]

The dot pattern formation typically takes place when the ion beam anisotropy is suppressed, which can be achieved by using a normal incidence or an oblique incidence with a simultaneous target rotation.[11,12,33] The only exception was the dot pattern observed on Ge surfaces irradiated with Xe^+ ions at 2 keV at a 20° angle of incidence. The authors attributed the hexagonal dot pattern to the increment in the ion incidence angle which enhanced the anisotropy in the curvature-dependent sputtering and promoted the formation of a hexagonal array of dots in accordance with an anisotropically generalized version of the damped nonlocal Kuramoto–Sivashinsky equation. The damping mechanism can be explained by a redeposition of the material.[12] In our study, due to the polyatomic incident ion beam, the linear cascades and thermal spikes are produced simultaneously at the irradiated surface. These thermal spikes induce local melted zones (pools) and the subsequent quenching resulting in a dot pattern formation. This is consistent with Fig. 2, where islands of dots arise only in some areas of the surface, and as the thermal spike cascade increases (ion fluence), the islands dimension and quantity also increases.

C. Ion bombardment at 373 K

Figure 3 shows the irradiated Ge surface for the target temperature of 373 K and ion fluence of 6.3×10^{16} [Fig. 3(a)] and 3.8×10^{17} ions/cm^2 [Fig. 3(b)]. In the case of the low ion fluence, the agglomeration of nanodots occurs, and the FFT spectra demonstrate a random distribution. There is a formation of islands of dots for the higher ion fluence [the top image in Fig. 3(b)]. The increase in the density of islands of dots is related to the ion fluence since the thermal spikes also increases. Nevertheless, the islands' density is much higher at high temperature (HT) than at RT [Fig. 2(d)]. A magnified image of the surface is shown in the bottom panels. The bottom left panel presents the AFM images with a size of 2 × 2 μm^2, and the bottom right panel shows the corresponding FFT images. In Fig. 3(b), the dot structures with no particular orientation on the surface are observed, the FFT image demonstrates a random distribution of dots; the average dot size is 55.9 nm. We attribute the islands of dots to an intermediate sputtering regime between the linear collision cascade and thermal spikes. This conjecture will be considered in detail below.

D. Ion bombardment at 573 K

When the target temperature was raised to 573 K, a dot pattern with a uniform distribution was observed over the

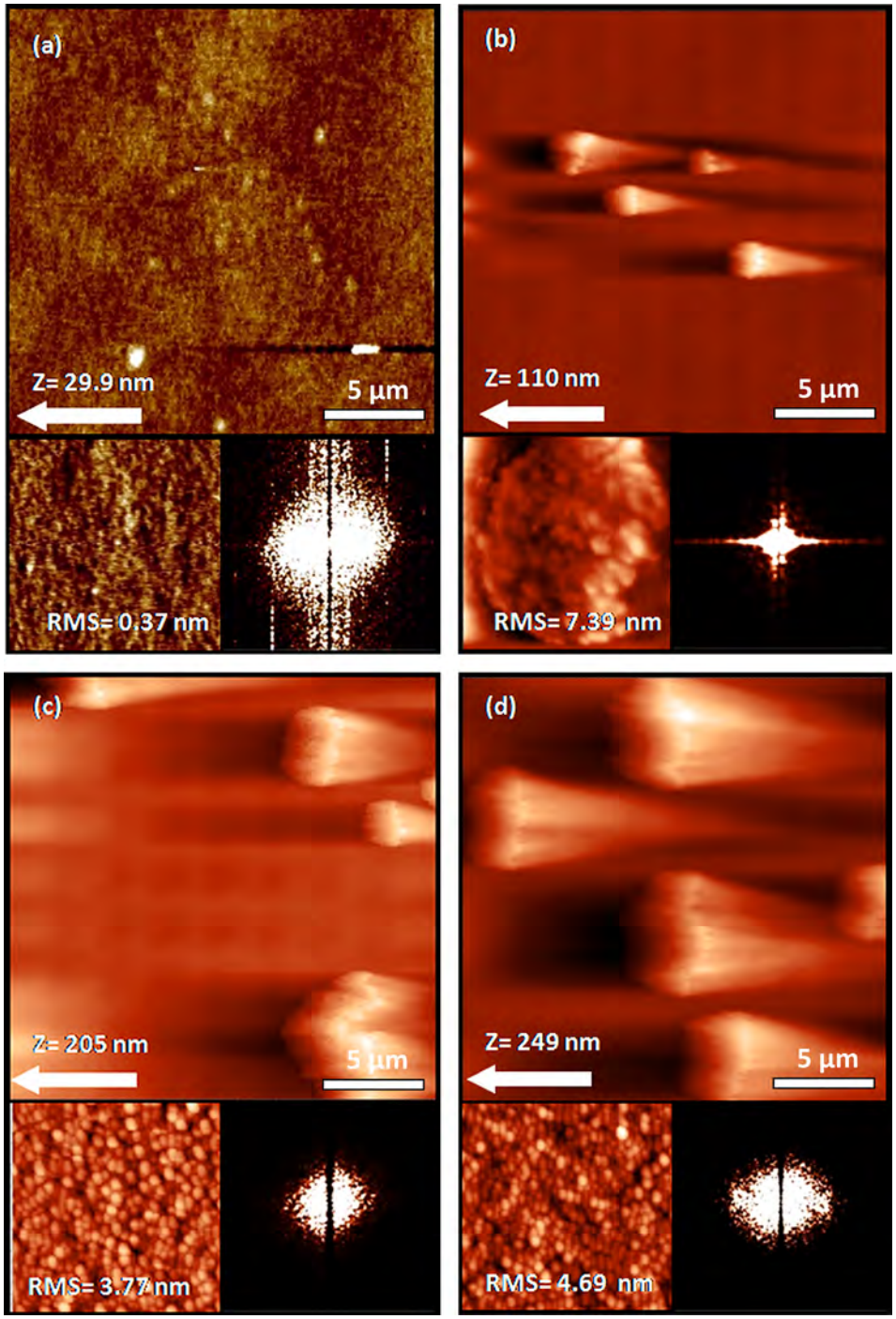

FIG. 2. (Color online) AFM images, top: $20 \times 20\ \mu m^2$; bottom: $2 \times 2\ \mu m^2$ (left) and the corresponding FFT image (right). Morphology of Ge surface after bismuth irradiation at room temperature for $E_{ion} = 30$ keV and $\theta_{inc} = 45°$. The ion fluence is different in each case: 6.3×10^{16} (a), 1.3×10^{17} (b), 2.5×10^{17} (c), and 3.8×10^{17} ions/cm^2 (d). The white arrow shows the projected ion beam direction. RMS is the root mean square roughness measured in a $5 \times 5\ \mu m^2$ area.

entire irradiated area since the rise in temperature induces an increment of the local melted zones. Figure 4 shows the irradiated surface for two different ion fluences: 6.3×10^{16} [Fig. 4(a)] and 3.8×10^{17} ions/cm^2 [Fig. 4(b)]. In the first case (the low ion fluence), the early stage of dot formation takes place. As the ion fluence increases, a distinct dot shape is formed. The average dot size is 68 nm. As one can see from the images shown in Figs. 2(c), 2(d), and 3(b), there is a correlation between the target temperature and the dot size. A similar relation between the dot size and target temperature was reported by Frost *et al.*[34] for InP sputtered by Ar^+ ions. The FFT image shows a preferential orientation of the dot pattern. As the target temperature increases, the density of the islands of dots become higher and higher, and eventually, the entire surface becomes covered with the dot structures. The disorder array of nanodots arises on the surface due to the quenching of the melted zones caused by the thermal spike cascades; this will be discussed below in detail.

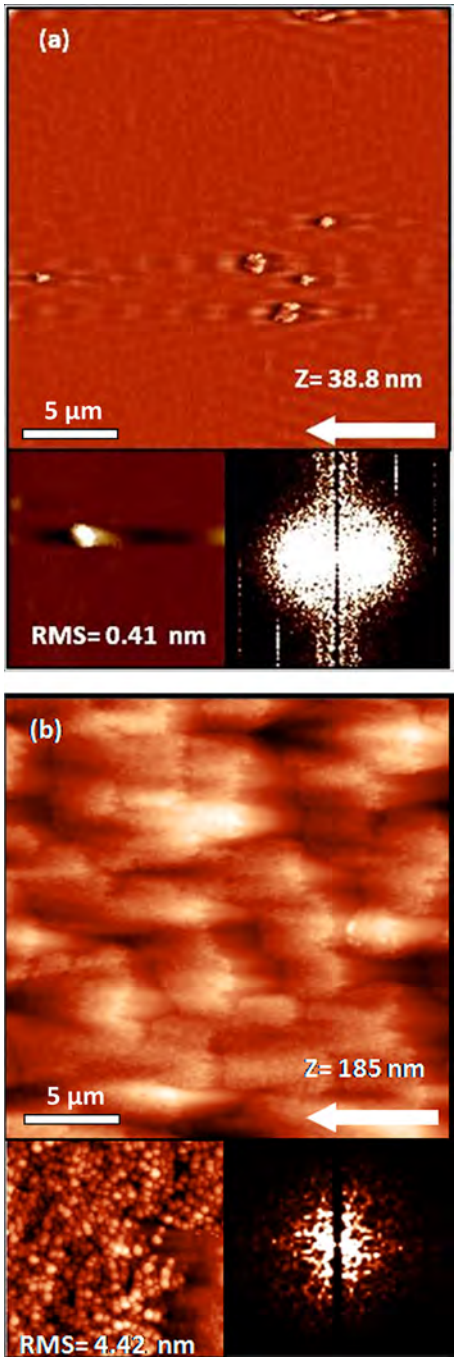

FIG. 3. (Color online) AFM images, top: 20 × 20 μm^2; bottom: 2 × 2 μm^2 (left) and the corresponding FFT image (right). Morphology of Ge surface after bismuth irradiation for $E_{ion} = 30$ keV, $\theta_{inc} = 45°$ and ion fluence of 6.3 × 10^{16} (a) and 3.8 × 10^{17} ions/cm^2 (b) at 373 K. The white arrow shows the projected ion beam direction. RMS is the root mean square roughness measured in a 5 × 5 μm^2 area.

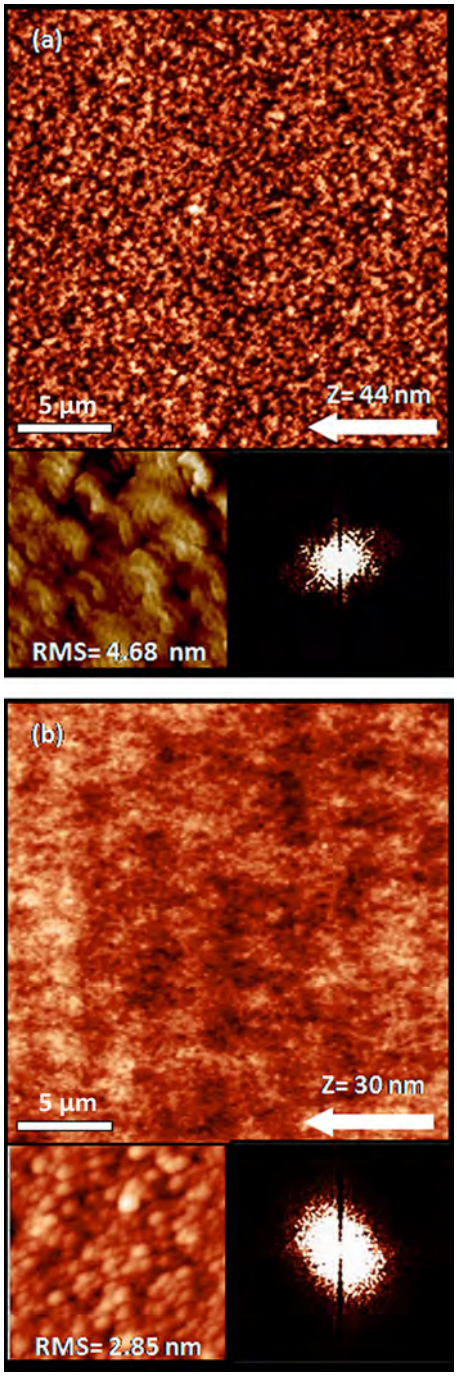

FIG. 4. (Color online) AFM images, top: 20 × 20 μm^2; bottom: 2 × 2 μm^2 (left) and corresponding FFT image (right). Morphology of Ge surface after bismuth irradiation for $E_{ion} = 30$ keV, $\theta_{inc} = 45°$ and ion fluence of 6.3 × 10^{16} (a) and 3.8 × 10^{17} ions/cm^2 (b) at 573 K. The white arrow shows the projected ion beam direction.

E. Ion bombardment at 773 K

The morphology of the structures obtained after bismuth bombardment at the target temperature of 773 K appreciably differs from the morphology of the structures obtained at lower target temperatures. Figure 5 shows the so-called checkerboard patterns of the irradiated Ge surfaces at different ion fluences: 1.3 × 10^{16} (a), 1.3 × 10^{17} (b), 2.5 × 10^{17} (c), and 3.8 × 10^{17} ions/cm^2 (d). Figure 5(a) presents the early stage of the checkerboard pattern. For ion fluencies above 1.3 × 10^{17} [Fig. 5(b)] the pattern is well defined. The average distance between the neighboring structures is 404.6, 412.5, and 454.8 nm, respectively. As shown by statistical analysis of the checkerboard pattern, the average length of the structures is 174, 208, and 227 nm, respectively. The average width is 60.2, 68.6, and 72.7 nm, respectively.

As mentioned in the Introduction, the Au_x^- cluster ion sputtering of an In metal target with an ion energy of 10 keV

results in a thermal spike regime of sputtering. So, there is every reason to believe that we definitely achieve the thermal spike regime with a more energetic Bi_x^+ polyatomic ion beam at a target temperature of 773 K. We suggest that at this temperature a "complete" surface recrystallization occurs due to a dominance of thermal spikes in a "competition" with the surface amorphization process induced by ion irradiation. Thus, the Ehrlich–Schwoebel barrier arises and, as a consequence, the preferential diffusion of adatoms and vacancies occurs due to the anisotropy of the crystalline surface, which results the checkerboard pattern.[18] This behavior agrees with the checkerboard morphology presented in Fig. 5 which shows a combination of pits (vacancies) and mounds (interstitial defects).

The checkerboard pattern was observed earlier[17,18,35] on Ge surfaces irradiated by an Ar^+ ion beam at 1 keV with a normal incidence with respect to the surface. In the work of Chowdhury *et al.*,[18] the energy of Ar^+ ion beam was in the limit of energy for sputtering. Their objective of irradiating the surface was only to produce defects and adatoms on the surface. However, in the work of Ou *et al.*,[17] the energy beam of 1 keV should cause amorphization of the irradiated surface. Nevertheless in their work, the crystalline checkerboard pattern is obtained for a substrate temperature of 528, 548, and 623 K, and the authors claim that the pattern is mainly related to the substrate temperature. Accordingly with Ou *et al.*,[17] there is a temperature window for the checkerboard pattern formation: above the recrystallization temperature and low enough to establish an ES barrier. In our case, this pattern was observed only when the substrate temperature was 773 K even for a low ion fluence of 1.3×10^{16} ions/cm^2, which corresponded to 60 s of erosion time. Figure 6(a) presents the checkerboard pattern obtained by argon irradiation,[17] and Fig. 6(b) shows the checkerboard pattern obtained in our study. It is evident that there are many similarities between the patterns even if the experimental conditions considerably differ. This is a strong indication that the thermal spikes regime of sputtering occurs also under sub-kilo-electron-volt ion irradiation, and this will be discussed below. In other hand, we should mention the results obtained by Bischoff *et al.*[19] when the irradiation of germanium surfaces by using Bi_1^+ ion beam with energy of 30 keV was performed in order to study the target temperature effect in the pattern formation. In their work, the target temperature was varied from 573 up to 773 K. At temperatures of 573 K, a spongelike structure was observed, whereas for a target temperature of 673 K, a dot pattern arose in the surface. Most important, in their experiment for a target

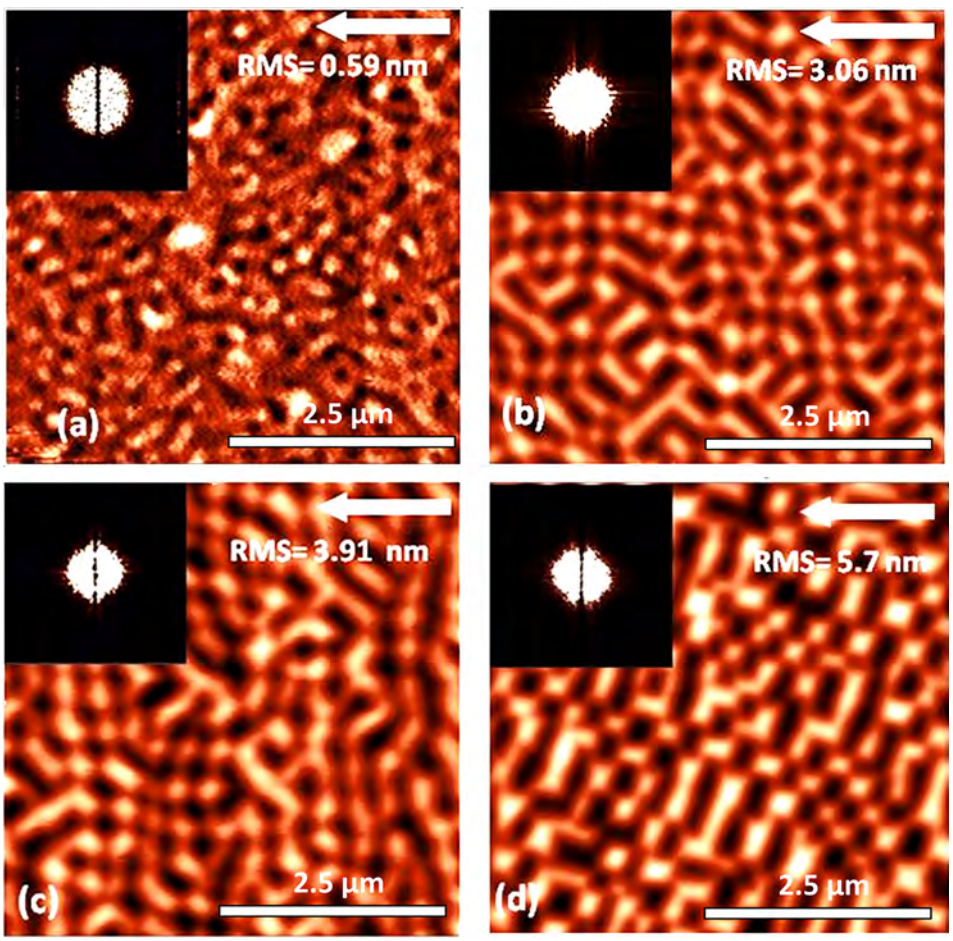

FIG. 5. (Color online) AFM images of $5 \times 5\ \mu m^2$ of Ge after bismuth irradiation at 773 K for $E_{ion} = 30$ keV and $\theta_{inc} = 45°$. The ion fluence is different for each case: 1.3×10^{16} (a), 1.3×10^{17} (b), 2.5×10^{17} (c), and 3.8×10^{17} ions/cm^2 (d). The inset shows corresponding Fourier images. The white arrow shows the projected ion beam direction. RMS is the root mean square roughness measured in a $5 \times 5\ \mu m^2$ area.

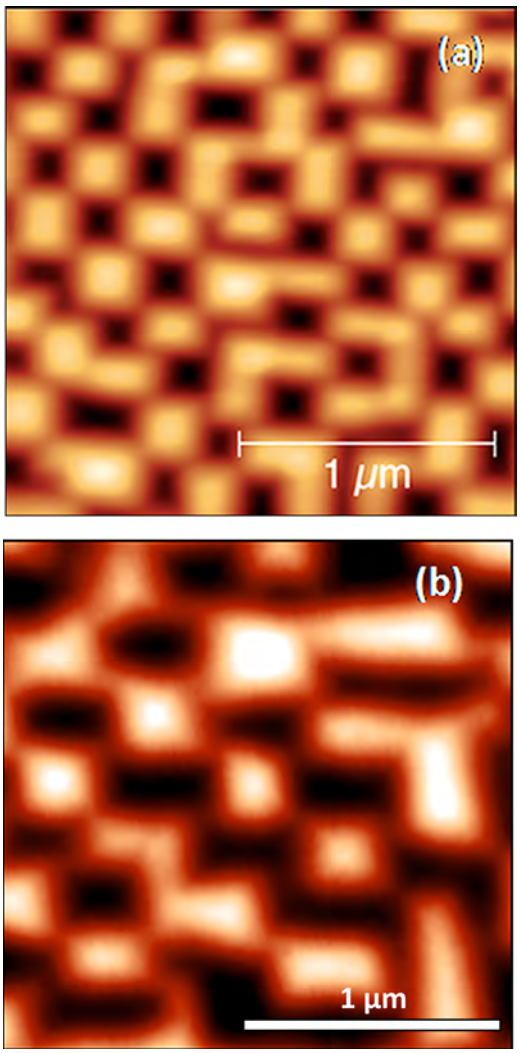

FIG. 6. (Color online) Checkerboard pattern on Ge surfaces produced by IBS under different experimental conditions. (a) The results obtained by Ou *et al*. (Ref. 17) for normal Ar^+ incidence at 1 keV. (b) The results obtained in our experiment in a micrograph $2 \times 2\ \mu m^2$. The ion dose is 3.8×10^{17} ions/cm^2, and the energy beam of Bi_m^+ is 30 keV at incidence of 45° with respect to the surface normal.

temperature of 773 K, the surface became smooth after the bismuth irradiation. This is contradictory to the concept that the checkerboard pattern depends strongly to the surface temperature (above recrystallization temperature) and the creation of defects by IBS.

F. Raman analysis

Since the irradiated area is too small ($300 \times 300\ \mu m$) to study the structural properties by XRD, micro Raman spectroscopy was applied for a crater bottom analysis. Raman spectroscopy was used to analyze the target chemical composition and also to compare the amorphous and crystalline phases of the ion irradiated Ge, since the Raman spectra of the phases differ in the peak shape and position.[36]

Figure 7 shows normalized Raman spectra for Ge bombarded with bismuth ions and also for the nonirradiated surface. The contributions of amorphous Ge at 160.8 and 269.5 cm^{-1} are observed for low temperatures and also for

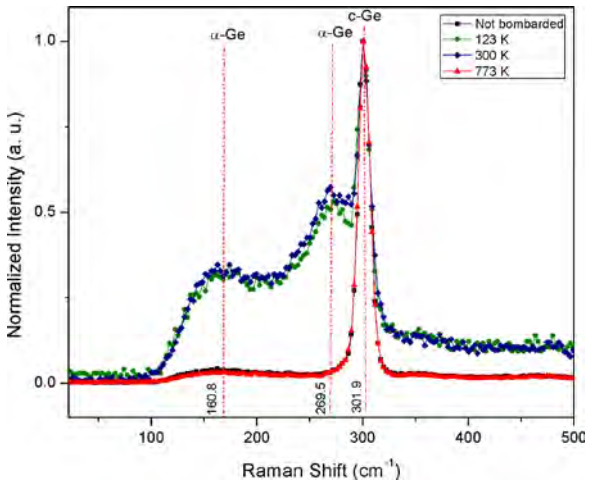

FIG. 7. (Color online) Raman spectra of nonbombarded and irradiated Ge at different substrate temperatures: 173, 300, and 773 K. The spectra were taken at the center of sputter craters.

the room-temperature Ge substrate. We consider here the formation of a thin surface amorphized layer due to ion irradiation, as the linear cascade model predicts. However, the Raman spectrum of the irradiated Ge at 773 K shows the vibration mode of crystalline Ge that is identical to the no irradiated crystal. This result indicates that a complete (or almost complete) recrystallization of the thin near-surface layer takes place. This recrystallization process is related to a dominance of thermal spike cascades melting and recrystallization processes with respect to the amorphization process caused by ion irradiation.

G. Effect of thermal spikes on the pattern formation dynamics

The discussion of the pattern formation dynamics at elevated temperatures typically involves the consideration of two regimes of ion sputtering, i.e., the linear collision cascade regime and the thermal spike regime. Moreover, we assume that both mechanisms can occur simultaneously under definite conditions. Then, we assume a preferable linear cascade regime in the case of low-temperature Bi^+ ion sputtering when a smooth surface is observed. At room temperature, we detect a number of "islands" of nanodots, which increases (the number of islands and their size) with the fluence and temperature growth up to the moment when the entire sputtered area is covered with nanodots. We invoke the "partial" thermal spike regime in order to explain the formation of islands of nanodots. The local melted zones are formed in the thermal spike regime due to dissipation of the primary ion energy in local areas resulting in an excess of the target melting temperature in these zones. Quenching of these melting zones gives rise to the nanodots formation in the near-surface layer. It is important to note here that this scenario is a conventional description of grain growth in different metals and semiconductors which occurs under the mega-electron-volt ion irradiation when the thermal spike formation does not raise any doubts. See, for example, the publications of Kaoumi *et al*.[37] (with the references

therein[1–14]) and Marks.[38] The ion irradiation process is a statistical process. This means that at room temperature and up to 373 K, we can consider a "mixture" of cascades, a part of which corresponds to linear cascades, but another part corresponds to thermal spikes. Therefore, there is a competition between the amorphization process of a near-surface thin layer caused by primary ion collisions and the recrystallization and the formation of nanocrystals in local melting zones (spikes). This idea is presented schematically in Fig. 8. At time t_0, the surface bombardment gives rise to a partial amorphization, and the formation of melting zones (as a result of thermal spike formation) inside the amorphized layer takes place. At time t_1 (a few picoseconds after the spike formation), some of these melting zones are recrystallized, and the erosion process continues as the incoming ions impinge on the surface. This leads to the removal of the material, and recrystallized zones emerge on the surface. The surface relief which is demonstrated schematically for time t_2 is a result of a "selective sputtering" of the "composite" near-surface layer and consists of crystalline nanoparticles embedded in an amorphous matrix. A temperature growth leads to an increase in the number of thermal spikes and, as a consequence, the area is covered with islands of nanodots. When the major part of the cascades corresponds to the thermal spike regime, a thin quasiliquid film is formed on the irradiated surface, and a complete recrystallization of a near surface layer occurs. The checkerboard structure in Figs. 5 and 6 demonstrates the results of ion beam interaction with such a recrystallized surface where the Ehrlich–Schwoebel barrier should be taken into account for the diffusion of adatoms and vacancies, formed due to ion irradiation.[18]

The above described model is very similar to the one suggested by Bischoff *et al.*,[20] but has some differences. In our model, we do not limit the formation of nanodots by quenching of melting pools formed by heavy cluster ions with a relatively high energy (>25 keV) only. We believe that a part of atomic ions can form thermal spikes due to a statistical character of the ion–solid interaction process, and (or) under favorable conditions like an elevated temperature of the target. Moreover, we extend the model to the ion sputtering performed by the ultralow energy ions (0.5–5 keV), see below.

The similarity between the reliefs obtained under considerably differing regimes (see Fig. 6) leads to some important conclusions. In the case of Bi^+ ion sputtering, the Raman spectra of Fig. 7 do not show a vibration mode associated with bismuth or Bi_xGe_{1-x}, and there is no critical surface composition change for Ar^+ ion sputtering as well. Therefore, any binary target sputtering effect can be excluded from the consideration of the checkerboard pattern formation. A strong difference in the angles of incidence of primary ions (45° for the Bi^+ ion beam and normal incidence for Ar^+ ions[17]) and an appreciable difference in the primary ion energy (30 keV for Bi^+ ions and 1 keV for Ar^+ ions) allow us to exclude both these parameters from the consideration as well. Thus, we can conclude that the amorphization of the top surface layer, its partial and then complete recrystallization at elevated temperatures and under the thermal spike regime of sputtering are the main and, probably, the only reasons for the surface pattern dynamics from the smooth surface, through the nanodots pattern and finally to the checkerboard relief formation.

The conclusions made above means, among other things, that 1 keV Ar^+ ion sputtering of a Ge target at 528 K corresponds to the thermal spike regime, while there is a mixture of linear cascades and thermal spikes at room-temperature Ar^+ ion sputtering of Ge. This conclusion contradicts the conventional notion of the ion sputtering process,[27] according to which the low-energy sputtering corresponds to the so-called "knock-on" sputtering regime. It is assumed that in this sputtering regime, only a few collisions between a primary ion and target atoms take place instead of a real cascade generation.

In our earlier work,[39] we put forward another hypothesis on the low-energy ion sputtering process (<3 keV). We considered the release of primary ion energy in a cascade volume and concluded that a decrease in the ion energy from 5 to 0.5 keV, for example, resulted in a radical increase in the energy density released per unit volume, or per atom of the target in the cascade. Indeed, we could estimate the cascade volume, V, in the first approximation by using the projected

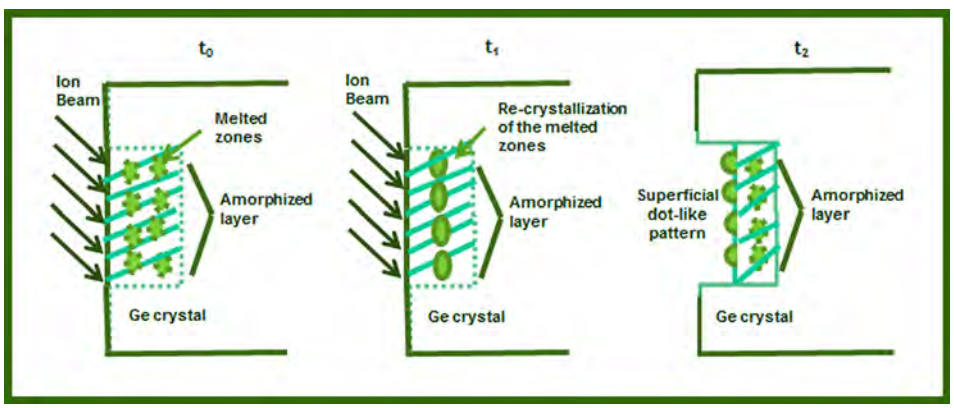

FIG. 8. (Color online) Schematic diagram of surface morphology modification under ion irradiation in the presence of a mixture of linear cascades and thermal spikes.

range, R_p, of primary ions, which is estimated, in its turn, for the low primary ion energy E_0 as[40]

$$R_p = C_l(\mu)M_2\left[\left(\frac{Z_1^{\frac{2}{3}}+Z_2^{\frac{2}{3}}}{Z_1Z_2}\right)E_0\right]^{\frac{2}{3}}, \quad (1)$$

where M_2 is the target atom mass, and Z_i is the atomic number of target atoms (2) and primary ion (1), respectively.

The density of the energy dispersed in the cascade per unit volume (or per atom) is proportional to the primary ion energy and inversely proportional to the cascade volume (V): $\delta E \sim Eo/V \sim E_0/(R_p)^3$. Then, we obtain from Eq. (1) that the power density δE in the cascade is proportional to $\sim 1/E_0$ for the low-energy regime of sputtering. Therefore, we can conclude that nonlinear effects can arise as the ion irradiation energy becomes lower than approximately 5 keV. Of course, we consider here medium mass and heavy ion sputtering of dense targets.

The nonlinear effects in the target under sub-kilo-electron-volt ion sputtering will be considered in detail in a separate paper. Here, we only note that computer simulations show that the local temperature in a cascade can exceed the melting temperature of the target in the case of irradiation by primary ions with the energy from 500 to 5000 eV,[40] and references therein: [2.65–67, 2.87–88].

According to common view, atoms in a collision cascade can leave the solid if they are close to the surface (they are in first two monoatomic layers) and have energy greater than the surface binding energy (SBE). The SBE value is varied between 2 and 5 eV; thus, the high energy secondary particles ($E > 20$ eV) represent the recoil energy distribution in the collision cascade. This is the reason why the energy distribution of sputtered particles is used to separate the linear cascade and thermal spike sputtering regimes in practice.[28]

In Ref. 41, the authors demonstrated the energy distribution of the secondary Ag^+ ions sputtered from a silver target by 6 keV Xe^+ ions and conclude the thermal spike regime for this experiment.

In the work of Mousel *et al*. is shown the energy distribution of Cu atoms sputtered from copper by Ar^+ ion with different ion energies.[42] It is evident that the well-known Sigmund–Thompson distribution, which is typical for the linear cascades sputtering regime, can be used to describe the energy distribution of Cu atoms observed for 1030 eV sputtering alone. When sputtering energy is below 1 keV, the exponentially decaying distribution is observed, which is typical for thermal spike sputtering regime. So, we have the experimental confirmation of the thermal spike regime for the ultralow energy ion sputtering.

But if it is true, the nanodot formation under low-energy Ar^+ and Xe^+ ions at a normal incidence reported in a series of articles[10–12,22–24] can be explained by the suggested above mechanism (see also Fig. 8): a mixture of "linear" and "nonlinear" cascades is formed in these experiments; the nonlinear cascades (thermal spikes) result in formation of nanocrystals due to recrystallization of melted zones. Continuous ion sputtering of such nanocrystals can be observed on the irradiated surfaces of GaSb,[10] InP,[9] and Ge.[17]

Recently, El-Atwani *et al*.[43] successfully applied the model of Bischof *et al*.,[20] describing the resolidification of the melted zones formed by primary cluster ions, for explanation of nanodots patterns formation on III–V semiconductors irradiated by 0.5 keV noble gas ions. Unfortunately, the authors have not shown in detail the course of reasoning used to justify the use of the melted pools model for the ultralow energy sputtering. But it is evident that they considered the thermal spike sputtering concept in their speculation.

IV. CONCLUSIONS

The patterns formed on the bismuth ion irradiated surface of the Ge target at different temperatures have been studied. According to the experimental data, the thermal spike regime of sputtering was found to dominate at 573 K. We attributed the formation of the nanodot pattern over the entire surface to this effect. For a target temperature of 773 K, a checkerboard pattern which was very similar to that obtained earlier under radically differing experimental conditions was observed. The crystalline surface effect in adatoms and vacancies diffusions results in the formation of the checkerboard structure on such surface. The differences in the experimental conditions for the formation of a checkerboard pattern let us suggest that morphology is independent of the angle of incidence of the primary ion and also of the ion type, energy, fluence, and the surface composition. The major conclusions are as follows:

(1) The Ge surface relief formed under Bi^+ ion sputtering strongly depends on the target temperature and ranges from a flat surface at 123 K to the checkerboard pattern for the target sputtered at 773 K. We conclude that the observed patterns are the result of only crystalline structure of the surface being under ion irradiation. Indeed, there is not any preferential diffusion effect for adatoms and vacancies on the totally amorphized surface at 123 K target temperature. Together with a very short diffusion length for surface adatoms and vacancies, this leads to the smooth surface formation. On the other hand, when a part of primary ions produce thermal spikes at the surface, solidification of the melted zones results in the formation of the nanodots pattern. When the number of thermal spikes (melted zones) exceeds a critical value, a complete recrystallization of the ion irradiated surface occurs. This "crystalline structure" mechanism lets us to explain the similar surface pattern dynamic observed for Ge target for very different experimental regimes: Bi_n^+ 30 keV ion sputtering (this work and in Ref. 20), 0.4–0.5 keV Ne^+, Ar^+, Kr^+, and Xe^+ sputtering.[42]

(2) Bi^+ ion sputtering of Ge at room temperature and up to 573 K corresponds to a "mixed" sputtering regime, when a part of the cascades generated by primary ions corresponds to linear cascades and the other part corresponds to thermal spikes. In our opinion, this regime of sputtering results in the formation of nanodots on the irradiated surface which are observed experimentally for the sub-kilo-electron-volt

sputtering regime of GaSb, GaP, Si, InP, Ge, etc. It is important to note that if our suggestion is correct, the regime of nanodot patterning can be realized for almost any material and almost any primary ion when a correct target temperature is chosen.

(3) The surface smoothing can be induced by sample rotation among other techniques. However, the LN cooling is a good alternative to be used in the FIB sample preparation and depth profiling analysis by SIMS and related analytical techniques. Since it results in a flat sample surface and avoids an increase in surface roughness during the ion sputtering process enhancing the resolution of the depth profiles.

ACKNOWLEDGMENT

The authors would like to thank the Mexican National Council for Science and Technology (CONACYT Reg. 271128) for supporting this work financially, Project No. CB-2012/176179.

[1]M. V. R. Murty, Surf. Sci. **500**, 523 (2002).
[2]C. Hofer, C. Teichert, M. Oehme, J. Werner, K. Lyutovich, and E. Kasper, Appl. Surf. Sci. **256**, 267 (2009).
[3]K. Elst, A. Adriaens, and F. Adams, Int. J. Mass Spectrom. Ion Processes **171**, 191 (1997).
[4]R. M. Bradley and J. M. E. Harper, J. Vac. Sci. Technol., A **6**, 2390 (1988).
[5]G. Carter and V. Vishnyakov, Phys. Rev. Lett. B **54**, 17647 (1996).
[6]D. Flamm, F. Frost, and D. Hirsch, Appl. Surf. Sci. **179**, 95 (2011).
[7]T. K. Chini, D. P. Datta, and S. R. J. Bhattacharyya, Phys.:Condens Matter **21**, 224004 (2009).
[8]E. Chason, T. M. Mayer, B. K. Kellerman, D. T. McIlroy, and A. Howard, J. Phys Rev. Lett. **72**, 3040 (1994).
[9]A. Karen, K. Okun, F. Soeda, and A. Ishitani, J. Vac. Sci. Technol., A **9**, 2247 (1991).
[10]S. W. Maclaren, J. E. Baker, W. L. Finnegan, and C. M. Loxton, J. Vac. Sci. Technol., A **10**, 468 (1992).
[11]S. Facsko, T. Dekorsy, C. Koerdt, C. Trappe, H. Kurz, A. Vogt, and H. L. Hartnagel, Science **285**, 1551 (1999).
[12]B. Ziberi, F. Frost, and B. Rauschenbach, Appl. Phys. Lett. **88**, 173115 (2006).
[13]M. Paniconi and K. R. Elder, Phys. Rev. E **56**, 2713 (1997).
[14]J. M. García, M. Castro, and R. Cuerno, Phys. Rev. Lett. **96**, 086101 (2006).
[15]M. Teichmann, J. Lorbeer, B. Ziberi, F. Frost, and B. Rauschenbach, New J. Phys. **15**, 103029 (2013).
[16]S. A. Mollick, D. Ghose, P. D. Shipman, and R. M. Bradley, Appl. Phys. Lett. **104**, 043103 (2014).
[17]X. Ou and S. Facsko, Nucl. Instrum. Methods B **341**, 13 (2014).
[18]D. Chowdhury, D. Ghose, and S. A. Mollick, Vaccum **107**, 23 (2014).
[19]L. Bischoff, W. Pilz, and B. Schmidt. Appl. Phys. A **104**, 1153 (2011).
[20]L. Bischoff, K. H. Heinig, B. Schmidt, S. Facsko, and W. Pilz, Nucl. Instrum. Methods, B **272**, 198 (2012).
[21]L. Bischoff, R. Böttger, P. Philipp, and B. Schmidt, "Nanostructures by mass-separated FIB," in *FIB Nanostructures*, Lecture Notes in Nanoscale Science and Technology Vol. 20, edited by Z. Wang (Springer, Berlin, 2013), pp. 465–525.
[22]R. Böttger, L. Bischoff, K.-H. Heinig, W. Pilz, and B. Schmidt, J. Vac. Sci. Technol., B **30**, 06FF12 (2012).
[23]R. Böttger, A. Keller, L. Bischoff, and S. Facsko, Nanotechnology **24**, 115702 (2013).
[24]R. Böttger, K.-H. Heinig, L. Bischoff, B. Liedke, R. Hübner, and W. Pilz, Phys. Status Solidi RRL **7**, 501 (2013).
[25]R. Böttger, K.-H. Heinig, L. Bischoff, B. Liedke, and S. Facsko, Appl. Phys. A **113**, 53 (2013).
[26]P. Sigmund, J. Mater. Sci. **8**, 1545 (1973).
[27]P. Sigmund, "Sputtering by ion bombardment: Theoretical concepts," in *Sputtering by Particle Bombardment I*, edited by R. Behrisch (Springer-Verlag, Berlin, 1981), p. 18.
[28]A. V. Samartsev, A. Duvenbeck, and A. Wucher, Phys. Rev. B **72**, 115417 (2005).
[29]S. Mammeri, S. Ouichaoui, H. Ammi, C. A. Pineda-Vargas, A. Dib, and M. Msimanga, Nucl. Instrum. Methods B **354**, 235 (2015).
[30]Yu. Kudriavtsev, A. Hernández, R. Asomoza, S. Gallardo, M. López, and K. Moiseev, "SIMS depth profiling of 'frozen' samples: In search of ultimate depth resolution regime," Surf. Interface Anal. (published online).
[31]J. Muñoz-García, L. Vázquez, R. Cuerno, J. A. Sánchez-García, M. Castro, and R. Gago, Toward Funct. Nanomater. **5**, 323 (2009).
[32]M. Engler, S. Macko, F. Frost, and T. Michely, Phys. Rev. B **89**, 245412 (2014).
[33]F. Frost, A. Schindler, and F. Bigl, Phys. Rev. Lett. **85**, 4116 (2000).
[34]F. Frost, B. Ziberi, T. Hoche, and B. Rauschenbach, Nucl. Instrum. Methods B **216**, 9 (2004).
[35]X. Ou, A. Keller, M. Helm, J. Fassbender, and S. Facsko, Phys. Rev. Lett. **111**, 016101 (2013).
[36]L. S. Taylor and G. Zografi, Pharm. Res.**15**, 755 (1998).
[37]D. Kaoumi, A. T. Motta, and R. C. Birtcher, J. Appl. Phys. **104**, 073525 (2008).
[38]N. A. Marks, Phys. Rev. B: Condens. Matter **56**, 2441 (1997).
[39]Yu. Kudriavtsev and R. Asomoza, "Sub-keV ion sputtering: Is it really 'knock-on' regime?," in *18th International Conference on Secondary Ion Mass Spectrometry*, Riva del Garda, Trentino, Italy, 18–23 September (2011).
[40]H. Gnaser, "Low-energy ion irradiation of solid surfaces," in *Springer Tracts in Modern Physics*, edited by G. Höhler (Springer Verlag, Berlin, 1999), Vol. 146, p. 13.
[41]M. Szymoński and A. E. De Vries, Phys. Lett. A **63**, 359 (1977).
[42]T. Mousel, W. Eckstein, and H. Gnaser, Nucl. Instrum. Methods B **152**, 36 (1999).
[43]O. El-Atwani, S. A. Norris, K. Ludwig, S. Gonderman, and J. P. Allain, Sci. Rep. **5**, 18207 (2015).